

Cite this: *Dalton Trans.*, 2026, **55**, 3967

Beyond bond distances: a purely geometrical descriptor correlating with covalency-related bonding terms

Jorge Pardos,^a Jorge Gonzalo,^b Pedro Merino^a and Jorge Echeverría^{*b}

Quantifying covalency remains a central challenge in understanding chemical bonding. Traditional distance–bond strength correlations often fail in diverse bonding regimes, and most existing metrics require computationally demanding electronic structure analyses. Here we introduce the penetration index, a purely geometrical, size-normalized descriptor derived from atomic positions and covalent/van der Waals radii, which is related to covalency. For a broad set of systems, including diatomic molecules and ions, phosphine chalcogenides, hydrogen- and halogen-bonded complexes, and halonium ions, the penetration index shows remarkably strong correlations (R^2 up to 0.99) with established computational covalency descriptors such as ΔE_{SC} in bonded-ALMO-EDA, V_{XC} in IQA, ΔE_{CT} in ALMO-EDA, DDEC6 bond orders, and 3c–4e bonding percentages. In all cases, it outperforms bare interatomic distances, transforming scattered trends into linear relationships. The penetration index thus offers a robust, low-cost, and transferable structural metric that correlates with covalency-related bonding terms for both covalent and noncovalent interactions.

Received 11th November 2025,
Accepted 10th February 2026

DOI: 10.1039/d5dt02699g

rsc.li/dalton

1. Introduction

It is no exaggeration to say that all of chemistry is built on the concept of chemical bonding. Among the various types of bonding interactions, the covalent bond represents a fundamental mode of atomic binding, forming the basis for molecular architecture in chemistry, biology, and materials science. Since the publication of Linus Pauling's seminal book,¹ which laid the cornerstone for our modern understanding of chemical bonding, the concept of the covalent bond has remained at the center of theoretical chemistry. Over the decades, successive refinements have given rise to two major theoretical frameworks that coexist to this day.² Although they essentially describe the same underlying phenomenon, they diverge in their interpretations and emphases. Thus, despite more than half a century of advances, we still lack a unified and transparent view of the true nature of the covalent bond. If we focus on how to determine the nature of a chemical bond, quantifying covalency remains a nontrivial challenge, particularly in

complex systems where electron delocalization, polarization, or partial ionic character complicate simplistic interpretations.

Traditionally, the quantification of covalency in chemical bonds (*i.e.*, measuring the extent to which two atoms share electrons) has been approached from several theoretical and computational perspectives. For instance, different bond order indices have been derived from electron density-based methods, such as Mayer Bond Order,³ which is based on density matrix and accounts for orbital overlap, Wiberg Bond Index (WBI), derived from natural atomic orbitals and commonly used in Natural Bond Orbital (NBO) analysis,⁴ or the Delocalization Index (DI), that measures electron sharing between atomic basins within the Quantum Theory of Atoms in Molecules (QTAIM).⁵ On the other hand, Energy Decomposition Analysis (EDA) schemes separate energy into components usually including an orbital term that accounts for the covalent contribution.⁶ Within Molecular Orbital methods, the degree of covalency can be inferred from orbital compositions, overlap populations or bonding *vs.* antibonding orbital occupancy, while Valence Bond Theory can directly quantify contributions from covalent and ionic resonance structures.⁷ Experimentally, K-edge X-ray Adsorption Spectroscopy (XAS) has served to quantify metal–ligand covalency in transition metal complexes⁸ or π covalency in halogen bonding.⁹

From a structural point of view, covalency has traditionally been related to bond distance, assuming that decreasing the

^aInstituto de Biocomputación y Física de Sistemas Complejos (BIFI) and Departamento de Química Orgánica, Universidad de Zaragoza, Pedro Cerbuna 12, 50009 Zaragoza, Spain

^bInstituto de Síntesis Química y Catálisis Homogénea (ISQCH) and Departamento de Química Inorgánica, Facultad de Ciencias, Universidad de Zaragoza, Pedro Cerbuna 12, 50009 Zaragoza, Spain. E-mail: jorge.echeverria@unizar.es



bond distance increases the bond energy and, thus, the degree of covalency. However, this bond length/bond strength correlation has found to be not applicable in many chemical systems.^{10,11} In this context, the development of geometrically derived descriptors, which rely on nuclear positions and atom sizes, offers a promising way toward low-cost and broadly applicable measures of bonding characteristics. The recently introduced penetration index exemplifies this paradigm, providing a size-corrected metric of interatomic proximity that can qualitatively differentiate between van der Waals, noncovalent, and covalent regimes.^{12,13} However, a more systematic and quantitative linkage between geometry and covalency remains underexplored.

Here, we demonstrate that the penetration index between the two atoms involved in a chemical bond nicely correlates with many different calculated parameters used to quantify covalency. Remarkably, the use of penetration index significantly improves the corresponding linear correlations with respect to raw interatomic distances. Accordingly, the penetration index serves as a geometrical parameter that captures bonding trends associated with covalency in both chemical bonds and noncovalent interactions.

2. Methods

Interatomic contacts

To investigate interatomic contacts, we employed the recently developed penetration index (p).^{12,14} This metric quantifies the extent of spatial overlap between two atoms, A and B, and is defined as follows:

$$p_{AB} = 100 \cdot (v_A + v_B - d_{AB}) / (v_A + v_B - r_A - r_B) \quad (1)$$

where d_{AB} denotes the interatomic distance between atoms A and B, while r and v correspond to the covalent¹⁵ and van der Waals¹⁶ radii, respectively. When the interatomic distance equals the sum of the van der Waals radii, p_{AB} is 0%. As the atoms approach one another and reach a separation equal to the sum of their covalent radii, p_{AB} increases to 100% (Fig. 1). Intermediate distances yield values between 0% and 100%, reflecting varying degrees of noncovalent or weakly covalent interaction, whereas values of $p_{AB} > 100\%$ indicate separations shorter than the sum of the covalent radii, and values below 0% correspond to distances exceeding the van der Waals threshold. The penetration index offers a distinct advantage over the use of raw interatomic distances, as it introduces a chemically intuitive framework to assess atomic proximity and interpenetration, independent of atomic nature.¹⁷

To estimate the quality of linear correlation we use the coefficient of determination R^2 , which is a statistical measure that represents the proportion of the variance in the dependent variable that is predictable from the independent variable and defined as the square of the Pearson correlation coefficient (r).

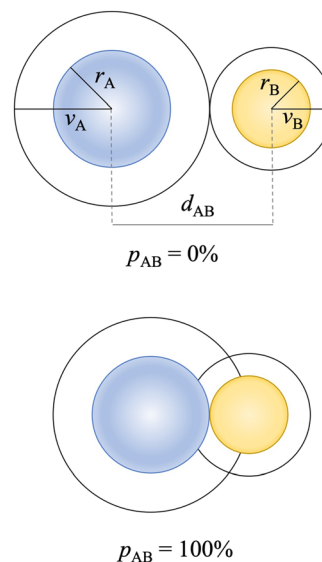


Fig. 1 Illustration of the scenario in which two atoms, A (blue) and B (yellow), are (above) in contact at a separation equal to the sum of their van der Waals radii ($d_{AB} = v_A + v_B$), resulting in no interpenetration and a penetration index $p_{AB} = 0\%$, and (below) separated by a distance equal to the sum of their covalent radii ($d_{AB} = r_A + r_B$), corresponding to complete interpenetration and a penetration index $p_{AB} = 100\%$.

Quantification of covalency

For the analysis of X=P double bonds in X=PR₃ (X = S, Se, Te; R = H, Me, ⁱPr, Ph) phosphine chalcogenide derivatives, we performed Interacting Quantum Atoms (IQA) calculations. The IQA method¹⁸ decomposes the interaction energy between two atoms in the real space into two terms, one associated with coulombic (V_{Cl}) and the other with exchange–correlation (V_{XC}) interactions. Thus, we use the V_{XC} energy term (between X and P) as an indicator of the bond covalency.¹⁹ IQA analysis was done with the AIMAll software on the corresponding B3LYP pseudo-single determinant Kohn–Sham wavefunctions obtained from B3LYP-D3BJ/Def2-TZVPP geometry optimizations.

Hydrogen-bonded systems ($H_2O \cdots H_2O$, $HF \cdots NH_3$, $H_2O \cdots NH_3$, $HF \cdots HF$, $H-F-H^-$, $H_2O \cdots OH^-$) and halonium compounds (I_3^- , $py \cdots [Cl-py]^+$, $py \cdots [Br-py]^+$, $py \cdots [I-py]^+$, $4-NH_2-py \cdots [I-(4-NH_2-py)]^+$, $4-NO_2-py \cdots [I-(4-NO_2-py)]^+$, $4-OH-py \cdots [I-(4-OH-py)]^+$) were analyzed with the second generation ALMO-EDA method,^{20,21} which decomposes the interaction energy between two fragments into several energy terms that are chemically meaningful ($\Delta E_{Int} = \Delta E_{Elec} + \Delta E_{Pauli} + \Delta E_{Disp} + \Delta E_{Pol} + \Delta E_{CT}$). Since covalent bonds involve the sharing of electrons, a process that includes a significant electron donation/back-donation mechanism, the charge transfer energy (ΔE_{CT}) is usually related to the degree of covalency of a given interaction.²² Calculations of hydrogen-bonded systems were done at the $\omega B97x-D/def2-TZVP$ level of theory, whereas data for halonium ions was taken from a previous publication at the MN12-SX/def2-TZVP level.²³



The study of single covalent bonds in X_2 and HX ($X = F, Cl, Br, I$) was carried out at the $\omega B97X-D/def2-TZVP$ level of theory by means of the Bonded-ALMO-EDA method.²⁴ The Bonded-ALMO-EDA scheme includes a spin-coupling energy term (ΔE_{SC}) that is due to electron pairing and loosely corresponds to the idea of covalency. For the computation of this energy, each half of the bond is initially computed as an isolated restricted open-shell system, constrained to the geometry it adopts within the final bonded complex. These fragments are then combined into a nonorthogonal supersystem in a high-spin triplet configuration by block-diagonal concatenation of their respective molecular orbitals. Subsequently, a spin-flip procedure is applied to generate a two-configurational wavefunction, yielding a spin-coupled state that retains the character of the original fragment orbitals. The associated energy change, denoted as ΔE_{SC} , is typically negative in the case of covalent bonding, reflecting the stabilizing nature of spin coupling. This spin-coupled system is then further relaxed by allowing orbital rotations between the doubly occupied and half-occupied orbitals, resulting in the final preparation of the fragments. All EDA analyses, both bonded and non-bonded, were performed with Q-Chem 6.²⁵

For the analysis of halogen-bonded neutral systems of the type $Y-X\cdots AR_m$ ($F_2\cdots OH_2$, $F_2\cdots NH_3$, $F_2\cdots SH_2$, $Cl_2\cdots OH_2$, $Cl_2\cdots NH_3$, $Cl_2\cdots SH_2$, $Cl_2\cdots PH_3$) and ionic systems ($[F\cdots F\cdots F]^-$, $[Cl\cdots Cl\cdots Cl]^-$, $[Br\cdots Br\cdots Br]^-$, $[F\cdots Cl\cdots F]^-$, $[F\cdots H\cdots F]^-$, $[F\cdots PH_2\cdots F]^-$, $FCl\cdots Cl^-$, $HCCl\cdots Cl^-$, $NCcl\cdots Cl^-$, $O_2NCl\cdots Cl^-$, $FH_2P\cdots Cl^-$, $FHS\cdots Cl^-$) we employed the data generated by Cremer *et al.*²⁶ The authors optimized the set of halogen-bonded systems at the CCSD(T)/aug-cc-pVTZ level and then obtained the bond strength orders (BSO) $n(XY)$ from the corresponding stretching force constants based on the generalized Badger rule derived by Cremer and co-workers.²⁷ Then, they estimated the percentage of three-center four-electron (3c-4e) bonding in the systems as the quotient between the X-A and X-Y BSOs (3c-4e percentage = $100 \times n(XA)/n(XY)$). Since the covalent character of a halogen bond increases as the interaction approaches a 3c-4e bonding regime (e.g. 100% 3c-4e bonding in $[F\cdots F\cdots F]^-$), the 3c-4e percentage can be used as an indication of how covalent a halogen bond is.

We also used the bond order as an indicator of covalency. Any bond order quantifies the number of electrons exchanged between two atoms in a chemical bond and, therefore, can be easily related to covalency. Bond order and bond length values for the investigated molecules BaX ($X = H, O, S, F, Cl, Br, I$), BX ($X = H, N, O, S, F, Cl, Br$), SiX ($X = H, N, O, S, Se, F, Cl$), NX ($X = H, O, S, F, Cl, Br$), PbX ($X = H, O, S, Se, Te, F, Cl, Br$), X_2 ($X = H, He, Li, Be, B, C, N, O, F, Ne, Na, Mg, Al, Si, P, S, Cl, Ar, K, Ca, Sc, Ti, V, Cr, Fe, Co, Ni, Cu, Zn, Ga, Ge, As, Se, Br, I, Kr, Rb, Sr, Y, Zr, Nb, Mo, Rh, Pd, Ag, Cd, In, Sn, Sb, Te, Xe, Cs, Ba, W, Ir, Pt, Au, Hg, Tl, Pb, Bi, Rn$) and ions (H_2^+ , HO^- , ClO^- , BC^- , CN^+ , CN^-) were taken from Manz and Chen.²⁸ In their work, they used the density derived electrostatic and chemical (DDEC6) method,²⁹ which assigns atomic electron and spin distributions to each atom in a chemical system, to calculate the bond orders of a large set of diatomic molecules.

3. Results and discussion

We first analyzed the bonding of two sets of diatomic molecules, namely halogens, X_2 , and hydrogen halides, HX , ($X = F, Cl, Br, I$) using Bonded-ALMO-EDA. The bonding energy was decomposed into its physical components, and the energy term associated with covalency (ΔE_{SC}) was found to correlate with bond length in each molecular set. Specifically, linear correlation analyses yielded R^2 values of 0.88 for X_2 and 0.90 for HX (Fig. 2A and C), indicating a strong dependence of ΔE_{SC} on bond length. Notably, when bond length was replaced by the penetration index, the linear correlations improved significantly, with R^2 values increasing to 0.99 and 0.96 for X_2 and HX , respectively (Fig. 2B and D).

To further evaluate the performance of the penetration index, we extended our analysis to systems featuring double bonds. Specifically, we investigated a series of twelve phosphine chalcogenides of the form $X=PR_3$ ($X = S, Se, Te$; $R = H, Me, ^iPr, Ph$). As Bonded-ALMO-EDA methods are currently limited in treating multiple bonds, we employed the Interacting Quantum Atoms (IQA) approach to decompose the bonding energy. Notably, when using the exchange-correlation energy term (V_{XC}) from IQA, the application of the penetration index transformed a reasonably good linear relationship based on bond lengths ($R^2 = 0.79$; Fig. 3A) into a highly linear correlation ($R^2 = 0.95$; Fig. 3B). It can be also seen that the greater the penetration, the more the absolute value of the V_{XC} energy term increases. These results reinforce the penetration index as a more sensitive and chemically meaningful descriptor of covalent bond strength than bond length alone, applicable to both single and double bonds. It is worth mentioning that the oxygen analogues, $O=PR_3$, were excluded since we observed

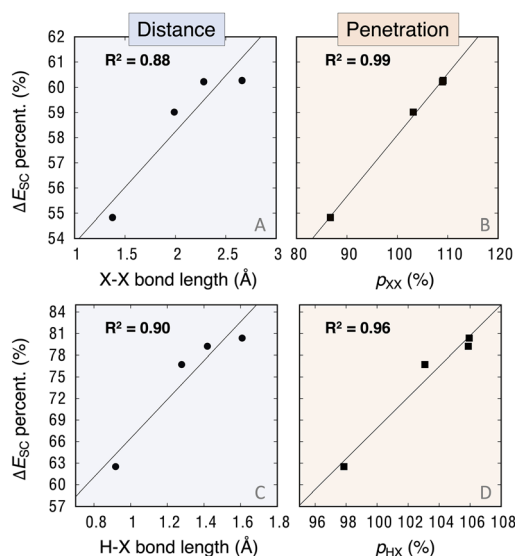


Fig. 2 Correlations between the bonded-ALMO-EDA spin-coupling energy term (ΔE_{SC} , expressed as the percentage with respect to the total attractive energy) and the bond distance (left) or penetration index (right) for (A and B) X_2 and (C and D) HX ($X = F, Cl, Br, I$) molecules.



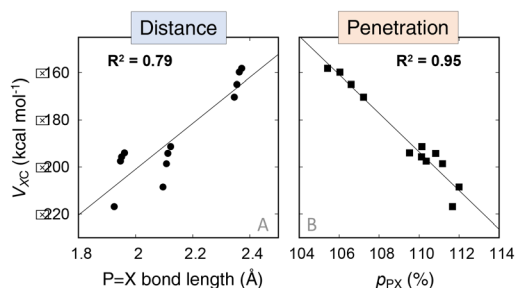


Fig. 3 Correlations between the IQA-derived exchange–correlation energy term (V_{XC}) and the (A) bond distance or (B) penetration index for the interaction of X and PR_3 in $X=PR_3$ (X = S, Se, Te; R = H, Me, 'Pr, Ph) molecules.

that they do not correlate with the IQA energy terms, probably due to the predominantly ionic character of the O–P bond.³⁰ Although the penetration index has been successfully applied to the analysis of purely ionic systems, the lack of correlation with energy terms from real-space IQA method for ionic bonds deserves further investigation.

Bond order (BO) is widely regarded as an indicator of the extent of covalent character in a chemical bond. In this context, we have utilized previously reported²⁸ BO values for various families of diatomic molecules, including BaX (X = H, O, S, F, Cl, Br, I), BX (X = H, N, O, S, F, Cl, Br), SiX (X = H, N, O, S, Se, F, Cl), NX (X = H, O, S, F, Cl, Br), and PbX (X = H, O, S, Se, Te, F, Cl, Br). These molecular families encompass a diverse range of atomic species, incorporating both metallic and non-metallic elements of different sizes and chemical characteristics. The graphical representation of these BOs *versus* the bond distance for each of these families leads to a series of scattered points with no clear trend (Fig. 4A, C, E, G and I). Notably, if we use the corresponding penetration indices instead of mere distances, a series of linear correlations appear with R^2 values of 0.85, 0.92, 0.93, 0.80 and 0.95 for BaX, BX, SiX, NX and PbX, respectively (Fig. 4B, D, F, H and J). Note that the particularly high penetration index values for BaX molecules are common for Ba containing systems due to the large size of this atom and also the partially ionic character of the Ba–X bond. Furthermore, in a set of 63 diatomic X_2 molecules, replacing bond distances with penetration indices enhances the correlation with bond order, raising R^2 from 0.50 to 0.74 (Fig. S1 in SI). It is noteworthy that, in all examined cases, greater degrees of penetration are associated with higher BO values.

In the molecular families examined thus far, one of the two atoms in each diatomic system has remained constant, while the other was systematically varied. We now extend our investigation to explore how penetration indices can be employed to assess the degree of covalency in systems where both atoms differ. For this purpose, we analyze a series of diatomic ions, namely H_2^+ , HO^- , ClO^- , BC^- , CN^+ , and CN^- . Plotting the bond order (BO) against bond length yields no significant correlation ($R^2 = 0.10$; Fig. 5A). In contrast, plotting BO against the

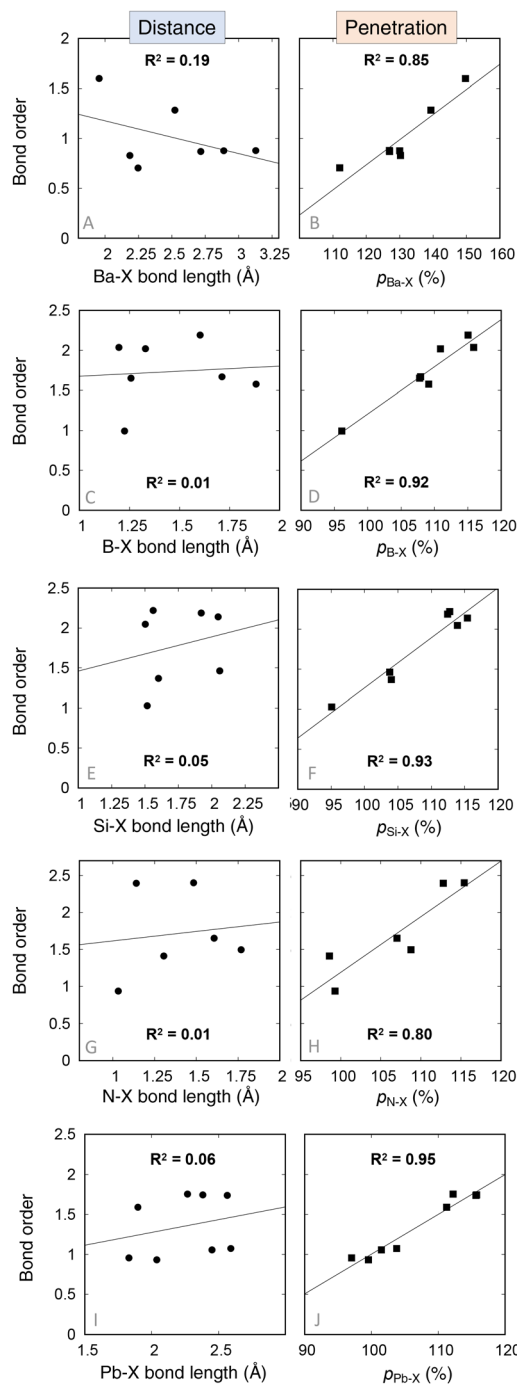


Fig. 4 Correlations between the computed DDEC6 bond orders and the bond distance (left) or penetration index (right) for different families of diatomic molecules: (A and B) BaX (X = H, O, S, F, Cl, Br, I); (C and D) BX (X = H, N, O, S, F, Cl, Br); (E and F) SiX (X = H, N, O, S, Se, F, Cl); (G and H) NX (X = H, O, S, F, Cl, Br); (I and J) PbX (X = H, O, S, Se, Te, F, Cl, Br).

penetration indices reveals a linear correlation, with a reasonably strong coefficient of determination ($R^2 = 0.73$; Fig. 5B). The absence of correlation between BO and bond length confirms that bond length alone is not a reliable indicator of



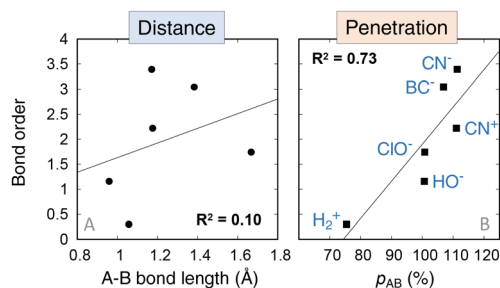


Fig. 5 Correlations between the computed DDEC6 bond orders and the (A) bond distance or (B) penetration index for a set of diatomic ions (H_2^+ , HO^- , ClO^- , BC^- , CN^- , CN^+).

covalent character in this context. Conversely, the maintenance of a good correlation between BO and penetration index in such diverse species highlights the robustness and transferability of the penetration index as a covalency probe. It is also worth noting that the penetration index, derived from covalent and van der Waals radii, effectively captures the degree of covalency even in ionic systems, consistent with previous findings involving other electronic descriptors.¹²

It is also of interest to evaluate the capacity of penetration indices to assess the degree of covalency in noncovalent interactions. Despite their classification, many interactions traditionally considered noncovalent, such as σ - and π -hole interactions, are known to exhibit a non-negligible degree of orbital overlap, indicating the presence of partial covalent character.^{31,32} We have selected a set of hydrogen-bonded systems ($\text{H}_2\text{O}\cdots\text{H}_2\text{O}$, $\text{HF}\cdots\text{NH}_3$, $\text{H}_2\text{O}\cdots\text{NH}_3$, $\text{HF}\cdots\text{HF}$, H-F-H^- , $\text{H}_2\text{O}\cdots\text{OH}^-$) and a set of halonium ions (I_3^- , $\text{py}\cdots[\text{Cl-py}]^+$, $\text{py}\cdots[\text{Br-py}]^+$, $\text{py}\cdots[\text{I-py}]^+$, $4\text{-NH}_2\text{-py}\cdots[\text{I-(4-NH}_2\text{-py)}]^+$, $4\text{-NO}_2\text{-py}\cdots[\text{I-(4-NO}_2\text{-py)}]^+$, $4\text{-OH-py}\cdots[\text{I-(4-OH-py)}]^+$) to be analyzed by means of ALMO-EDA. It is important to note that, in this type of energy decomposition analysis, the energetic contribution associated with inter-fragment orbital interactions is referred to as charge transfer (ΔE_{CT}). For hydrogen-bonded adducts, the linear correlation between the charge transfer term and the penetration index shows only a modest improvement when compared to the correlation with $\text{H}\cdots\text{X}$ distances, with the coefficient of determination (R^2) increasing from 0.89 to 0.96 (Fig. 6A and B). On the other hand, the bonding in halonium anions has been characterized as a halogen bond and is also commonly described within the framework of a three-center-four-electron (3c-4e) interaction.^{23,33} For the set of halonium ions examined, the relationship between the charge transfer (ΔE_{CT}) term and the interaction distance deviates significantly from linearity, primarily due to the triiodide ion (I_3^-) being markedly distant from the cluster of data points corresponding to the halonium cations ($R^2 = 0.12$; Fig. 6C). Notably, when the interaction distances are replaced by penetration indices, an almost perfect linear correlation is observed, which includes the I_3^- anion ($R^2 = 0.99$; Fig. 6D). This suggests that penetration indices are better predictors of electronic effects than internuclear distances, particularly when analyzing energetic contributions from orbital mixing in noncovalent interactions.

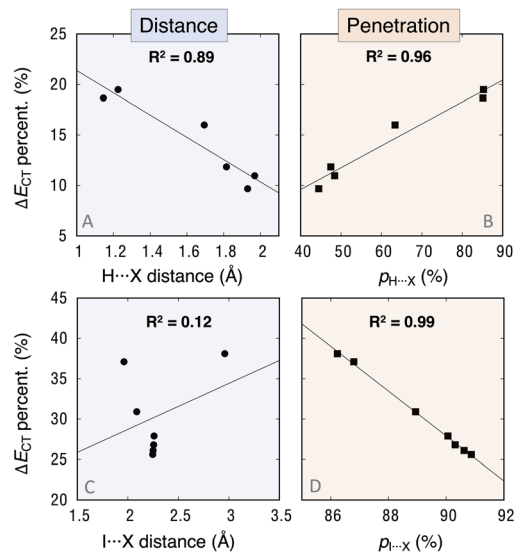


Fig. 6 Correlations between the ALMO-EDA charge transfer energy term (ΔE_{CT} , expressed as the percentage with respect to the total attractive energy) and the interatomic distance (left) or penetration index (right) for (A and B) hydrogen-bonded ($\text{H}_2\text{O}\cdots\text{H}_2\text{O}$, $\text{HF}\cdots\text{NH}_3$, $\text{H}_2\text{O}\cdots\text{NH}_3$, $\text{HF}\cdots\text{HF}$, H-F-H^- , $\text{H}_2\text{O}\cdots\text{OH}^-$) and (C and D) halogen-bonded (I_3^- , $\text{py}\cdots[\text{Cl-py}]^+$, $\text{py}\cdots[\text{Br-py}]^+$, $\text{py}\cdots[\text{I-py}]^+$, $4\text{-NH}_2\text{-py}\cdots[\text{I-(4-NH}_2\text{-py)}]^+$, $4\text{-NO}_2\text{-py}\cdots[\text{I-(4-NO}_2\text{-py)}]^+$, $4\text{-OH-py}\cdots[\text{I-(4-OH-py)}]^+$) systems.

Continuing the analysis of noncovalent interactions, we now turn our attention to two distinct sets of halogen-bonded systems: one composed of neutral species ($\text{F}_2\cdots\text{OH}_2$, $\text{F}_2\cdots\text{NH}_3$, $\text{F}_2\cdots\text{SH}_2$, $\text{Cl}_2\cdots\text{OH}_2$, $\text{Cl}_2\cdots\text{NH}_3$, $\text{Cl}_2\cdots\text{SH}_2$, $\text{Cl}_2\cdots\text{PH}_3$) and the other of ionic complexes ($[\text{F}\cdots\text{F}\cdots\text{F}]^-$, $[\text{Cl}\cdots\text{Cl}\cdots\text{Cl}]^-$, $[\text{Br}\cdots\text{Br}\cdots\text{Br}]^-$, $[\text{F}\cdots\text{Cl}\cdots\text{F}]^-$, $[\text{F}\cdots\text{H}\cdots\text{F}]^-$, $[\text{F}\cdots\text{PH}_2\cdots\text{F}]^-$, $\text{FCl}\cdots\text{Cl}^-$, $\text{HCCl}\cdots\text{Cl}^-$, $\text{NCCl}\cdots\text{Cl}^-$, $\text{O}_2\text{NCl}\cdots\text{Cl}^-$, $\text{FH}_2\text{P}\cdots\text{Cl}^-$, $\text{FHS}\cdots\text{Cl}^-$). In this context, the degree of covalency within the halogen bond is quantified in terms of the percentage contribution of the 3c-4e bonding character (values taken from ref. 27; see Methods section for details on the computational approach). In the case of neutral systems, no correlation is observed between the percentage of 3c-4e character and the interaction distance (Fig. 7A). However, when the 3c-4e contribution is plotted against the penetration index, a strong linear correlation emerges ($R^2 = 0.92$; Fig. 7B), indicating that increased orbital penetration corresponds to a greater 3c-4e character and, consequently, enhanced covalency of the halogen bond. For anionic systems, the improvement in correlation is more modest, with the coefficient of determination increasing from 0.57 (based on distances; Fig. 7C) to 0.75 (based on penetration indices; Fig. 7D). Nonetheless, a notable effect of using penetration indices is the reduced dispersion of systems exhibiting a purely covalent halogen bond (*i.e.*, 100% 3c-4e character), which now cluster more tightly around a penetration index value of $p_{\text{XA}} = 84\%$ (except for $[\text{F}\cdots\text{F}\cdots\text{F}]^-$, that remains at $p_{\text{XA}} = 66.3\%$).



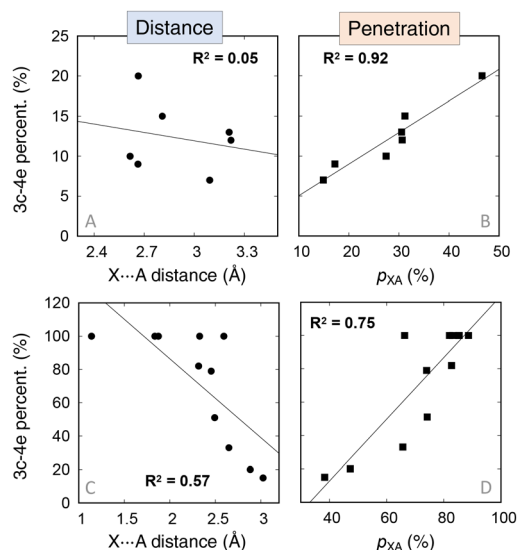


Fig. 7 Correlations between the 3c–4e character (as 3c–4e percentage) and the interatomic distance (left) or penetration index (right) for halogen-bonded (A and B) neutral systems of the type $Y-X\cdots AR_m$ ($F_2\cdots OH_2$, $F_2\cdots NH_3$, $F_2\cdots SH_2$, $Cl_2\cdots OH_2$, $Cl_2\cdots NH_3$, $Cl_2\cdots SH_2$, $Cl_2\cdots PH_3$) and (C and D) ionic systems ($[F\cdots F\cdots F]^-$, $[Cl\cdots Cl\cdots Cl]^-$, $[Br\cdots Br\cdots Br]^-$, $[F\cdots Cl\cdots F]^-$, $[F\cdots H\cdots F]^-$, $[F\cdots PH_2\cdots F]^-$, $FCl\cdots Cl^-$, $HCCl\cdots Cl^-$, $NCCl\cdots Cl^-$, $O_2NCl\cdots Cl^-$, $FH_2P\cdots Cl^-$, $FHS\cdots Cl^-$).

4. Conclusions

The penetration index, which incorporates both covalent and van der Waals radii, quantifies the effective interpenetration of atomic spheres, enabling direct comparison of interatomic separations in diverse chemical environments. In the present study, we have established the penetration index as a simple geometrical descriptor that assuredly captures the degree of covalency of chemical bonding.

The penetration index consistently outperforms bond distances in capturing the covalent character of chemical bonds for a broad range of systems. In purely covalent species, it shows nearly perfect linear correlations with computational covalency descriptors, including Bonded-ALMO-EDA spin-coupling energies (ΔE_{SC}) in diatomic molecules and IQA exchange–correlation energies (V_{XC}) in double bonds of phosphine chalcogenides, transforming otherwise scattered distance-based relationships into clear trends. Similar improvements are observed for DDEC6 bond orders in dozens of diatomic molecules and ions, where penetration values reveal a systematic increase in bond order with increasing covalent character. Importantly, the penetration index also succeeds in regimes traditionally classified as noncovalent. In hydrogen- and halogen-bonded complexes and halonium ions, it correlates strongly with ALMO-EDA charge transfer energies (ΔE_{CT})

	System	Method	Covalency parameter	R ² (Bond length)	R ² (Pen. Index)
Covalent	X ₂	Bonded-ALMO-EDA	ΔE_{SC}	0.88	0.99
	HX	Bonded-ALMO-EDA	ΔE_{SC}	0.90	0.97
	R ₃ P=X	IQA	V_{XC}	0.79	0.95
	BX	DDEC6	BO	0.01	0.92
	BaX	DDEC6	BO	0.19	0.85
	NX	DDEC6	BO	0.01	0.80
	SiX	DDEC6	BO	0.05	0.93
	PbX	DDEC6	BO	0.06	0.95
	Diatomic ions	DDEC6	BO	0.10	0.73
Non Covalent	X ₂	DDEC6	BO	0.50	0.74
	H-bonded	ALMO-EDA	ΔE_{CT}	0.89	0.96
	$[X-I\cdots X]^+$	ALMO-EDA	ΔE_{CT}	0.12	0.99
	X-bonded	Badger-Cremer	3c-4e (%)	0.05	0.92
	Ionic X-bonded	Badger-Cremer	3c-4e (%)	0.57	0.75

Fig. 8 Summary of all chemical systems analyzed in this work, including the computational method used for the analysis and the parameter used to quantify the degree of covalency. The determination coefficients (R^2) are given for the correlation of the covalency parameter versus bond distances and penetration indices.



and with the degree of three-center–four-electron (3c–4e) bonding. These results show that the penetration index cannot only be applied to covalent interactions but also captures the partial covalent character often hidden within weak intermolecular contacts. Fig. 8 summarizes the performance of the penetration index relative to raw interatomic distances in correlating covalency for all chemical systems and computational methods examined in this study.

In conclusion, the penetration index offers a general, transferable, and computationally affordable tool for examining chemical bonding allowing for the analysis of covalent and noncovalent interactions with a single descriptor. Accordingly, penetration indices can be used for high-throughput computational screening, logical molecular design, and the identification of structure–property relationships in complex molecular and material systems due to its simplicity and predictive ability.

Conflicts of interest

There are no conflicts to declare.

Data availability

The data supporting this article have been included as part of the supplementary information (SI). Supplementary information is available. See DOI: <https://doi.org/10.1039/d5dt02699g>.

Acknowledgements

This work was supported by projects PID2022-140244NB-I00 and PID2022-137973NB-I00, funded by MCIN/AEI/10.13039/501100011033 and by “ESF Investing in your future”, and Gobierno de Aragón (Grupo E34_23R).

References

- 1 L. Pauling, *The Nature of the Chemical Bond*, Cornell University Press, 1939.
- 2 G. Merino and T. Heine, *Angew. Chem., Int. Ed.*, 2015, **54**, 3551–3553.
- 3 I. Mayer, *J. Comput. Chem.*, 2007, **28**, 204–221.
- 4 F. Weinhold, *J. Comput. Chem.*, 2012, **33**, 2363–2379.
- 5 R. F. W. Bader, *Atoms in Molecules: A Quantum Theory*, Clarendon Press, 1994.
- 6 L. Zhao, M. von Hopffgarten, D. M. Andrada and G. Frenking, *Wiley Interdiscip. Rev.:Comput. Mol. Sci.*, 2018, **8**, e1345.
- 7 W. Wu, P. Su, S. Shaik and P. C. Hiberty, *Chem. Rev.*, 2011, **111**, 7557–7593.
- 8 K. Lee, A. V. Blake, C. M. Donahue, K. D. Spielvogel, B. J. Bellott and S. R. Daly, *Angew. Chem., Int. Ed.*, 2019, **58**, 12451–12455.
- 9 C. W. Kellett, P. Kennepohl and C. P. Berlinguette, *Nat. Commun.*, 2020, **11**, 3310.
- 10 B. A. Lindquist and T. H. Dunning, *J. Phys. Chem. Lett.*, 2013, **4**, 3139–3143.
- 11 M. Kaupp, D. Danovich and S. Shaik, *Coord. Chem. Rev.*, 2017, **344**, 355–362.
- 12 J. Echeverría and S. Alvarez, *Chem. Sci.*, 2023, **14**, 11647–11688.
- 13 J. Echeverría and S. Alvarez, *Struct. Bonding*, 2025, **190**, 263–296.
- 14 D. M. Gil, J. Echeverría and S. Alvarez, *Inorg. Chem.*, 2022, **61**, 9082–9095.
- 15 B. Cordero, V. Gómez, A. E. Platero-Prats, M. Revés, J. Echeverría, E. Cremades, F. Barragán and S. Alvarez, *Dalton Trans.*, 2008, 2832–2838.
- 16 S. Alvarez, *Dalton Trans.*, 2013, **42**, 8617–8636.
- 17 J. Echeverría and S. Alvarez, *Chem. Sci.*, 2024, **15**, 12166–12168.
- 18 M. A. Blanco, A. M. Pendás and E. Francisco, *J. Chem. Theory Comput.*, 2005, **1**, 1096–1109.
- 19 A. M. Pendás, J. L. Casals-Sainz and E. Francisco, *Chem. – Eur. J.*, 2019, **25**, 309–314.
- 20 P. R. Horn, Y. Mao and M. Head-Gordon, *J. Chem. Phys.*, 2016, **144**, 114107.
- 21 Y. Mao, P. R. Horn and M. Head-Gordon, *Phys. Chem. Chem. Phys.*, 2017, **19**, 5944–5958.
- 22 D. S. Levine and M. Head-Gordon, *Nat. Commun.*, 2020, **11**, 4893.
- 23 J. D. Velasquez, J. Echeverría and S. Alvarez, *Inorg. Chem.*, 2023, **62**, 8980–8992.
- 24 D. S. Levine and M. Head-Gordon, *Proc. Natl. Acad. Sci. U. S. A.*, 2017, **114**, 12649–12656.
- 25 E. Epifanovsky, A. T. B. Gilbert, X. Feng, J. Lee, Y. Mao, N. Mardirossian, P. Pokhilko, A. F. White, M. P. Coons, A. L. Dempwolff, Z. Gan, D. Hait, P. R. Horn, L. D. Jacobson, I. Kaliman, J. Kussmann, A. W. Lange, K. U. Lao, D. S. Levine, J. Liu, S. C. McKenzie, A. F. Morrison, K. D. Nanda, F. Plasser, D. R. Rehn, M. L. Vidal, Z.-Q. You, Y. Zhu, B. Alam, B. J. Albrecht, A. Aldossary, E. Alguire, J. H. Andersen, V. Athavale, D. Barton, K. Begam, A. Behn, N. Bellonzi, Y. A. Bernard, E. J. Berquist, H. G. A. Burton, A. Carreras, K. Carter-Fenk, R. Chakraborty, A. D. Chien, K. D. Closser, V. Cofer-Shabica, S. Dasgupta, M. de Wergifosse, J. Deng, M. Diedenhofen, H. Do, S. Ehlert, P.-T. Fang, S. Fatehi, Q. Feng, T. Friedhoff, J. Gayvert, Q. Ge, G. Gidofalvi, M. Goldey, J. Gomes, C. E. González-Espinoza, S. Gulania, A. O. Gunina, M. W. D. Hanson-Heine, P. H. P. Harbach, A. Hauser, M. F. Herbst, M. Hernández Vera, M. Hodecker, Z. C. Holden, S. Houck, X. Huang, K. Hui, B. C. Huynh, M. Ivanov, Á. Jász, H. Ji, H. Jiang, B. Kaduk, S. Kähler, K. Khistyayev, J. Kim, G. Kis, P. Klunzinger, Z. Koczor-Benda, J. H. Koh, D. Kosenkov, L. Koulias, T. Kowalczyk,



- C. M. Krauter, K. Kue, A. Kunitsa, T. Kus, I. Ladjánszki, A. Landau, K. V. Lawler, D. Lefrancois, S. Lehtola, R. R. Li, Y.-P. Li, J. Liang, M. Liebenthal, H.-H. Lin, Y.-S. Lin, F. Liu, K.-Y. Liu, M. Loipersberger, A. Luenser, A. Manjanath, P. Manohar, E. Mansoor, S. F. Manzer, S.-P. Mao, A. V. Marenich, T. Markovich, S. Mason, S. A. Maurer, P. F. McLaughlin, M. F. S. J. Menger, J.-M. Mewes, S. A. Mewes, P. Morgante, J. W. Mullinax, K. J. Oosterbaan, G. Paran, A. C. Paul, S. K. Paul, F. Pavošević, Z. Pei, S. Prager, E. I. Proynov, Á. Rák, E. Ramos-Cordoba, B. Rana, A. E. Rask, A. Rettig, R. M. Richard, F. Rob, E. Rossomme, T. Scheele, M. Scheurer, M. Schneider, N. Sergueev, S. M. Sharada, W. Skomorowski, D. W. Small, C. J. Stein, Y.-C. Su, E. J. Sundstrom, Z. Tao, J. Thirman, G. J. Tornai, T. Tsuchimochi, N. M. Tubman, S. P. Veccham, O. Vydrov, J. Wenzel, J. Witte, A. Yamada, K. Yao, S. Yeganeh, S. R. Yost, A. Zech, I. Y. Zhang, X. Zhang, Y. Zhang, D. Zuev, A. Aspuru-Guzik, A. T. Bell, N. A. Besley, K. B. Bravaya, B. R. Brooks, D. Casanova, J.-D. Chai, S. Coriani, C. J. Cramer, G. Cserey, A. E. DePrince III, R. A. DiStasio Jr., A. Dreuw, B. D. Dunietz, T. R. Furlani, W. A. Goddard III, S. Hammes-Schiffer, T. Head-Gordon, W. J. Hehre, C.-P. Hsu, T.-C. Jagau, Y. Jung, A. Klamt, J. Kong, D. S. Lambrecht, W. Liang, N. J. Mayhall, C. W. McCurdy, J. B. Neaton, C. Ochsenfeld, J. A. Parkhill, R. Peverati, V. A. Rassolov, Y. Shao, L. V. Slipchenko, T. Stauch, R. P. Steele, J. E. Subotnik, A. J. W. Thom, A. Tkatchenko, D. G. Truhlar, T. Van Voorhis, T. A. Wesolowski, K. B. Whaley, H. L. Woodcock III, P. M. Zimmerman, S. Faraji, P. M. W. Gill, M. Head-Gordon, J. M. Herbert and A. I. Krylov, *J. Chem. Phys.*, 2021, **155**, 084801.
- 26 V. Oliveira, E. Kraka and D. Cremer, *Phys. Chem. Chem. Phys.*, 2016, **18**, 33031–33046.
- 27 R. Kalescky, E. Kraka and D. Cremer, *J. Phys. Chem. A*, 2013, **117**, 8981–8995.
- 28 T. Chen and T. A. Manz, *RSC Adv.*, 2019, **9**, 17072–17092.
- 29 T. A. Manz, *RSC Adv.*, 2017, **7**, 45552–45581.
- 30 J. C. Pérez-Sánchez, C. Ceamanos, J. Echeverría, J. V. Alegre-Requena, R. P. Herrera and M. C. Gimeno, *Cell Rep. Phys. Sci.*, 2025, **6**, 102717.
- 31 S. J. Grabowski, *Chem. Rev.*, 2011, **111**, 2597–2625.
- 32 J. Echeverría, J. D. Velásquez and S. Alvarez, *Cryst. Growth Des.*, 2020, **20**, 7180–7187.
- 33 E. Adeniyi, F. E. Odubo, M. Zeller, Y. V. Torubaev and S. V. Rosokha, *Inorg. Chem.*, 2023, **62**, 18239–18247.

